

# Hybrid-loop servo control system of double toggle mechanical press for flexible forming process based on sliding mode control and neural network techniques

Jintao Liang, Shengdun Zhao, Yongqiang Zhao and Muzhi Zhu

## Abstract

A hybrid-loop servo control system based on sliding-mode control and neural network control is proposed in this article to realize flexible forming process on a double toggle mechanical press. First, kinematics and dynamic analysis of the drive system are conducted to derive the control objective behavior. Then, the structure of the hybrid-loop system is introduced; sliding-mode control is applied to compensate the punch position errors. In the inner loop of the servo motor, complementary sliding-mode control is used to track the motor rotation angle, and a radial basis function neural network estimator is applied to eliminate the considerable load disturbances in the stamping stage. Finally, experimental hardware is constructed and a compound blanking and drawing process is carried out to validate the proposed servo control system in practice. With different materials and drawing depth, high tracking accuracy and robustness are exhibited to realize favorable forming performance.

## Keywords

Hybrid-loop servo control, mechanical press, sliding-mode control, radial basis function neural network, stamping load

Date received: 30 May 2014; accepted: 7 September 2015

## Introduction

Mechanical presses are widely used in metal forming processes such as forging, extrusion, blanking, drawing, and bending. A new-generation mechanical press, which is called mechanical servo press, can be directly driven by alternating current (AC) servo motor, eliminating clutch, break, and large inertia flywheel. Compared to traditional presses, high efficiency, fast response, low noise, and energy consumption can be gained.<sup>1</sup> Furthermore, various complicated forming processes can be realized since the punch motion trajectory can be controlled flexibly by the servo motor, which would not only improve the dimensional accuracy and productivity effectively<sup>2</sup> but also eliminate forming defects,<sup>3</sup> extend die life, and reduce forming noise.<sup>4</sup>

In the servo press, appropriate transmission mechanisms between the motor and the punch should be designed to meet the stamping loadings and reduce the power demand of the motor.<sup>5,6</sup> Our research group has proposed a novel symmetrical double crank-toggle

mechanism and its optimization design in the previous works.<sup>7,8</sup> Then, the varied flexible forming processes are expected to be realized,<sup>9</sup> and this demands that the precision of punch motion should be maintained regardless of the diverse motion path of the punch and varying loadings. Consequently, a servo control system with favorable control technology and system architecture is required.

Sliding-mode control (SMC), for its rapid dynamic response and tough robustness to parameter variations and external disturbances, has been used to the field of mechanical and electric drives, such as robot manipulator,<sup>10</sup> switched reluctance motor,<sup>11</sup> and linear motor.<sup>12</sup>

Research Institute of Tool & Die Technology and Metal Forming, School of Mechanical Engineering, Xi'an Jiaotong University, Xi'an, P.R. China

## Corresponding author:

Jintao Liang, Research Institute of Tool & Die Technology and Metal Forming, School of Mechanical Engineering, Xi'an Jiaotong University, 28 Xianning West Road, Xi'an, Shaanxi 710049, P.R. China.  
 Email: topsteal@mail.xjtu.edu.cn

However, chattering phenomenon is unavoidable for the switching control. To eliminate chattering, a boundary layer around the switch surface is used usually, but it will bring indefinite steady-state error meanwhile. So, the complementary sliding-mode control (CSMC) has been developed,<sup>13,14</sup> which not only attenuates the chattering but also guarantees the steady-state precision. Furthermore, for the mechanical press, unknown high impact loading exists in the stamping stage, an intelligent control approach should be used to compensate this disturbance. Many researches about fuzzy control (FC),<sup>15–17</sup> neural network control (NNC),<sup>18–20</sup> and iterative learning control (ILC)<sup>21</sup> have been studied for adaptive compensators and dynamic observers. The radial basis function neural network (RBFNN), which has simple structure and fast convergence speed,<sup>22–24</sup> is one of the most effective intelligent compensation methods.

Several control systems on servo presses have been introduced in previous researches, for instance, a proportional derivative (PD)-type ILC controller for a hybrid-driven servo press was proposed by Cheng and Pei,<sup>25</sup> but the position controller and feedback controller were not discussed in detail, and the experiment results of drawing process were not perfect for obvious wrinkles existed. A fuzzy logic controller with self-tuning dead-zone compensation was proposed to control the punch motion of a switched reluctance motor direct-drive hydraulic press in Wei et al.,<sup>26</sup> full close-loop control was used because the control object was only a plunger cylinder. The tracking performance was discussed but no forming results of workpieces were shown. A double-axis servo system of small mechanical press was presented by Cheng et al.<sup>27</sup> for forming of small metal products, high precision and stable quality were gained as the forming force was low in the stamping stage.

Therefore, for the purpose of achieving various flexible forming processes on the double toggle mechanical press, a novel servo system should be developed and implemented practically, which can control the punch trajectories precisely against considerable stamping loads. Both tracking performance and processing quality should be researched in detail. For the nonlinear kinematics and dynamics of the transmission mechanisms, fully closed-loop control is difficult to realize. A novel hybrid-loop servo control system based on SMC and RBFNN is proposed in this article. Kinematics and dynamic analysis of the whole drive system are conducted to determine the control objective model. Then, the whole architecture of the servo system is presented, a feedforward controller is constructed for the conversion from the punch position to the motor rotation angle, and the SMC is applied to compensate the punch position errors. In the inner loop of the servo motor, CSMC is used to track the motor rotation angle. In addition, a RBFNN controller is applied to compensate the system uncertainties and the stamping impact load disturbances. Finally, the proposed servo control

system is implemented on the press prototype, and a compound blanking and drawing process is carried out for experimental validation. The results show that the proposed servo system is effective in maintaining favorable tracking precision and well forming quality against different materials and forming requirement.

## Kinematics and dynamics analysis of the drive system

The drive system of the double toggle mechanical press is the control objective of the servo control system, which is shown in Figure 1. A symmetrical structure is applied, in which a synchronizing gear mechanism is driven by the AC servo motor through a synchronous belt. Then, the synchronizing gears were connected to two crank-toggle mechanisms, respectively, to drive the

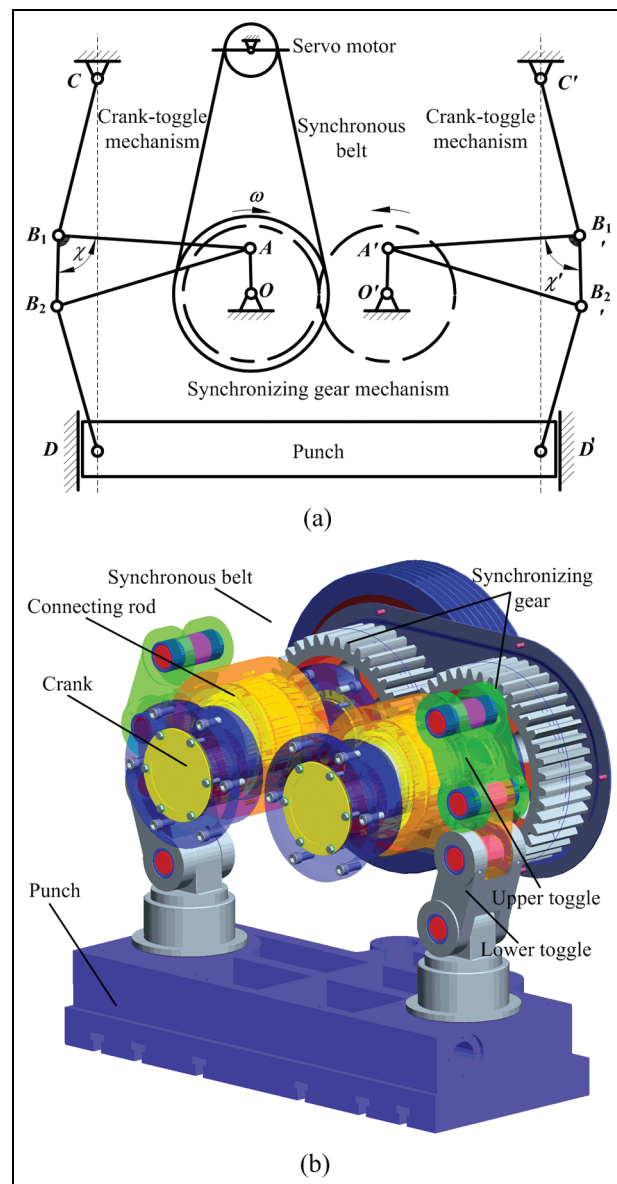


**Figure 1.** Drive system of the double toggle mechanical press: (a) schematic diagram and (b) transmission mechanism.

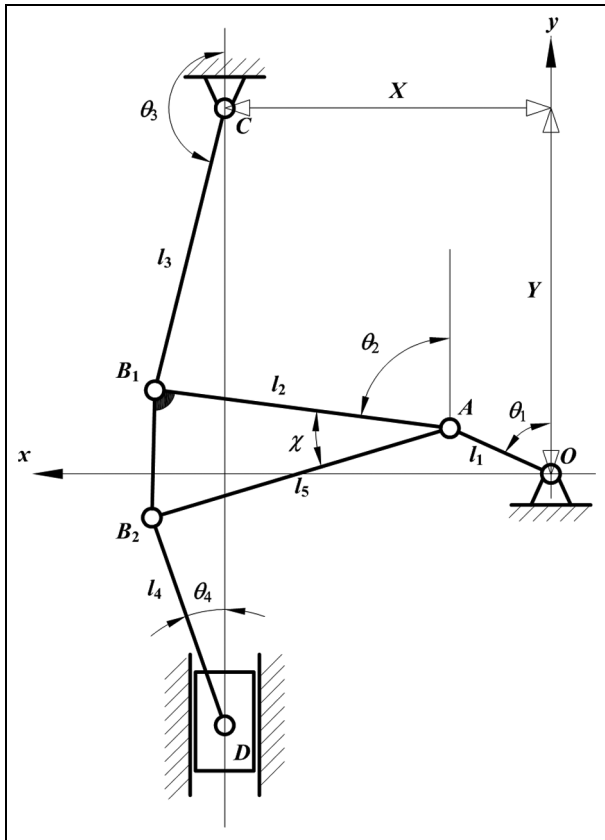


**Figure 2.** Kinematics analysis of drive system.

punch synchronously to achieve reciprocating motion for forming process.

The effective control of the punch trajectory is based on accurate kinematics and dynamics analysis of the drive system. For the symmetrical structure, only single-side mechanism is analyzed and the results would just be multiplied by 2. A planar coordinate system is built for kinematics analysis, the coordinate origin is the center of the crank shaft, as shown in Figure 2. According to the vector loop, two equations are obtained as follows

$$\begin{cases} l_1 \cos \varphi_1 + l_2 \cos \varphi_2 = Y + l_3 \cos \varphi_3 \\ l_1 \sin \varphi_1 + l_2 \sin \varphi_2 = X + l_3 \sin \varphi_3 \end{cases} \quad (1)$$

where  $l_1$ ,  $l_2$ , and  $l_3$  are the crank radius, the length of the connecting rod, and the length of the upper toggle, respectively;  $\varphi_1$ ,  $\varphi_2$ , and  $\varphi_3$  are the angles between the  $y$ -axis positive direction and the crank, the connecting rod, and the upper toggle, respectively. And  $X$  and  $Y$  are the dimensions between the center of the synchronizing gear and the rounded end of the press in the  $x$ - and  $y$ -axes direction, respectively. Three intermediate parameters  $E$ ,  $F$ , and  $G$  are defined, respectively, as

$$\begin{cases} E = Y - l_1 \cos \varphi_1 \\ F = X - l_1 \sin \varphi_1 \\ G = \frac{(X^2 + Y^2 + l_1^2 + l_3^2 - l_2^2 - 2Yl_1 \cos \varphi_1 - 2Xl_1 \sin \varphi_1)}{2l_3} \end{cases} \quad (2)$$

Then,  $\varphi_2$ ,  $\varphi_3$  and  $\varphi_4$  can be expressed as follows

$$\begin{cases} \varphi_3 = 2\text{atan}\left(\frac{F + \sqrt{E^2 + F^2 - G^2}}{E - G}\right) \\ \varphi_2 = \text{atan}\left(\frac{F + l_3 \sin \varphi_3}{E + l_3 \cos \varphi_3}\right) \\ \varphi_4 = \text{asin}\left(\frac{l_5 \sin(\varphi_2 + \chi) + l_1 \sin \varphi_1 - X}{l_4}\right) \end{cases} \quad (3)$$

where  $\varphi_4$  is the angle between the  $y$ -axis positive direction and the lower toggle;  $l_4$  and  $l_5$  are the length of the lower toggle and the consolidation rod, respectively; and  $\chi$  is the angle between the connecting rod and the consolidation rod.

Then, the coordinate point of the punch position can be expressed as

$$\begin{cases} D_{sx} = l_1 \sin \varphi_1 + l_5 \sin(\varphi_2 + \chi) - l_4 \sin \varphi_4 = X \\ D_{sy} = l_1 \cos \varphi_1 + l_5 \cos(\varphi_2 + \chi) - l_4 \cos \varphi_4 \end{cases} \quad (4)$$

Integrating equations (1)–(4), after the structure parameters ( $l_1$ ,  $l_2$ ,  $l_3$ ,  $l_4$ ,  $l_5$ ,  $X$ ,  $Y$ ,  $\chi$ ) are determined, the vertical position of the punch  $D_{sy}$  is only related to the crank input angle  $\varphi_1$ , and  $\varphi_1$  is the output value of the motor rotation angle  $\theta_m$  with the reduction ratio of the synchronous belt. So that the punch position can be controlled by  $\theta_m$  correspondingly. And  $\theta_m$  can be estimated referring to the field-oriented control (FOC) theory of the modern AC machines,<sup>28</sup> the motion equation of the servo motor can be expressed as follows

$$\begin{cases} J_e \frac{d^2 \theta_m}{dt^2} = K_T i_q - T_L - B_\omega \frac{d \theta_m}{dt} \\ K_T = \frac{3}{2} p \phi_{PM} \end{cases} \quad (5)$$

where  $J_e$  is the equivalent moment of inertia in the drive system,  $K_T$  is the torque coefficient,  $i_q$  is the stator  $q$ -axis current,  $T_L$  is the load torque,  $B_\omega$  is the viscous friction coefficient,  $p$  is the number of pole pairs, and  $\phi_{PM}$  is the flux linkage induced by the permanent magnets in the stator phases.

It can be seen that  $J_e$ ,  $K_T$ ,  $T_L$ , and  $B_\omega$  are not all constants in a punch stroke. System uncertainties and considerable external disturbances are different and unknown in different forming processes. Considering the parameter variations and loading disturbances, equation (5) can be rewritten as follows

$$\begin{aligned} \ddot{\theta}_m &= (a + \Delta a)\dot{\theta}_m + (b + \Delta b)i_q + (d + \Delta d)T_L \\ &= a\dot{\theta}_m + bi_q + \sigma \end{aligned} \quad (6)$$

where  $a = -B_\omega/J_e$ ,  $b = K_T/J_e$ , and  $d = -1/J_e$  represent the nominal values of the system parameters, and  $\Delta a$ ,  $\Delta b$ , and  $\Delta d$  are the corresponding parameter variations.  $i_q$  is the control effort, and  $\sigma$  represents the lumped uncertainty that

$$\sigma = \Delta a\dot{\theta}_m + \Delta b u + (d + \Delta d)T_L \quad (7)$$

Although impact load is existent,  $\sigma$  is bounded for energy conservation, and the upper bound  $\rho$  is defined as

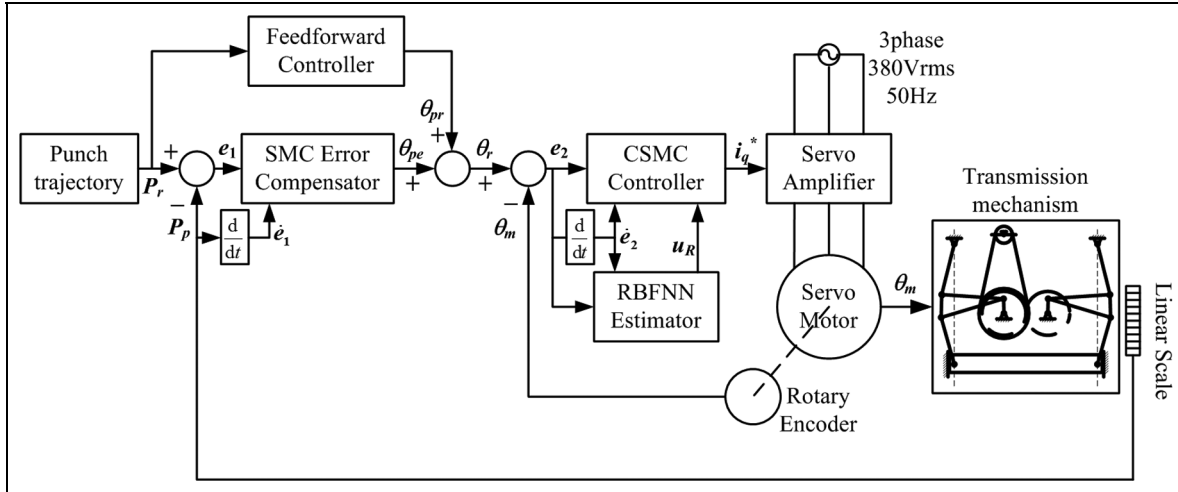


**Figure 3.** Schematic diagram of the hybrid-loop servo control system.

$$\rho = \max(|\sigma|) + \eta \quad (8)$$

where  $\eta$  is a positive constant.

## Hybrid-loop servo control system

To deal with the control objective as mentioned above, a hybrid-loop servo control system based on SMC and NNC is proposed in Figure 3. According to special forming process requirement, the punch trajectory is planned flexibly and transformed into the motor rotation angle reference  $\theta_{pr}$  through a feedforward controller employing equations (1)–(4), then an SMC is used to compensate the punch position errors brought by the mechanical errors of the transmission mechanisms, and then a CSMC with RBFNN estimator is applied to track the motor motion against the lumped uncertainties and stamping load. The control command of the CSMC is fed into the servo amplifier, which implements pulse width modulation (PWM) and FOC to drive the servo motor with the mechanical press transmission. Each control module is introduced in this section.

### SMC position error compensator

The position error of the punch is expressed as follows

$$e_1 = p_r - p_p \quad (9)$$

where  $p_r$  is the position command from the punch trajectory and  $p_p$  is the actual position of the punch measured by the linear scale. For compensating error in the outermost loop, conventional SMC is used to obtain fast response. The switching surface is selected as follows

$$s_1 = c_1 e_1 + \dot{e}_1 \quad (10)$$

where  $\dot{e}_1$  is the derivative of  $e_1$  and  $c_1$  is a positive constant, and the compensate effort  $\theta_{pe}$  is determined according to proportional switching control law

$$\theta_{pe} = (\alpha |e_1| + \beta |\dot{e}_1|) \text{sgn}(s_1) \quad (11)$$

where  $\alpha$  and  $\beta$  are positive constants.

### CSMC tracking controller

Tracking control is conducted in the closed-loop of the servo motor for energy supply and conversion, and the tracking error  $e_2$  and its derivative  $\dot{e}_2$  are defined as follows

$$\begin{cases} e_2 = \theta_r - \theta_m \\ \dot{e}_2 = \dot{\theta}_r - \dot{\theta}_m \end{cases} \quad (12)$$

where  $\theta_r$  is the rotation angle command combines the feedforward reference  $\theta_{pr}$  and the error compensation  $\theta_{pe}$  of the punch trajectory. CSMC is used to improve the servo tracking performance. According to Su and Wang<sup>13</sup> and Lin et al.,<sup>14</sup> the generalized SMC and its CSMC are defined, respectively, as follows

$$s_{2g} = \dot{e}_2 + 2\lambda e_2 + \lambda^2 \int_0^t e_2 d\tau \quad (13)$$

$$s_{2c} = \dot{e}_2 - \lambda^2 \int_0^t e_2 d\tau \quad (14)$$

where  $\lambda$  is a positive constant, and the relationship between the two switching surfaces is that

$$\dot{s}_{2g} = \dot{s}_{2c} + \lambda(s_{2g} + s_{2c}) \quad (15)$$

Then, equivalent control law can be designed as follows

$$u_e = \frac{1}{b} \left[ \ddot{\theta}_r - a\dot{\theta}_m + \lambda(2\dot{e}_2 + \lambda e_2 + s_{2g}) + \rho \text{sat} \left( \frac{s_{2g} + s_{2c}}{\Phi} \right) \right] \quad (16)$$

where

$$\text{sat}\left(\frac{s_{2g} + s_{2c}}{\Phi}\right) = \begin{cases} 1 & s_{2g} + s_{2c} \geq \Phi \\ \frac{s_{2g} + s_{2c}}{\Phi} & -\Phi < s_{2g} + s_{2c} < \Phi \\ -1 & s_{2g} + s_{2c} \leq -\Phi \end{cases} \quad (17)$$

is a saturation function used to suppress the chattering phenomenon. However, the upper bound  $\rho$  should contain the stamping load to guarantee in the stamping stage even it exists transitorily. Whereas  $\rho$  would cause significant chattering in other stages, so that adaptive algorithm is applied to estimate the lumped uncertainty  $\sigma$ .

### RBFNN estimator

RBFNN is a three-layer neural network which has been validated to represent any nonlinear functions with arbitrary precision. Therefore, a RBFNN estimator with two inputs and one output is used to compensate the lumped uncertainty.<sup>18</sup> Its structure is shown in Figure 4, which consists of input, hidden, and output layers.  $\mathbf{E} = [e_2, \dot{e}_2]$  is the input vector of RBFNN. In the hidden layer, the Gaussian function is chosen as the receptive-field function as follows

$$\varphi_j(\mathbf{E}) = \exp\left(-\frac{\|\mathbf{E} - \mathbf{c}_j\|^2}{2\kappa_j^2}\right) \quad j = 1, 2, \dots, L \quad (18)$$

where  $L$  is the number of nodes in the hidden layer, and  $\mathbf{c}_j$  and  $\kappa_j$  are the center vector and the width of the Gaussian function, respectively.  $\|\cdot\|$  is the Euclidean norm. Then, the output of the RBFNN is obtained by the weighted sum method and becomes the compensation of the CSMC as follows

$$\hat{u}_R = \sum_{j=1}^L \hat{\omega}_j \varphi_j(\mathbf{E}) \quad (19)$$

where  $\hat{\omega}_j$  is the connective weight between the hidden and the output layers; according to the universal

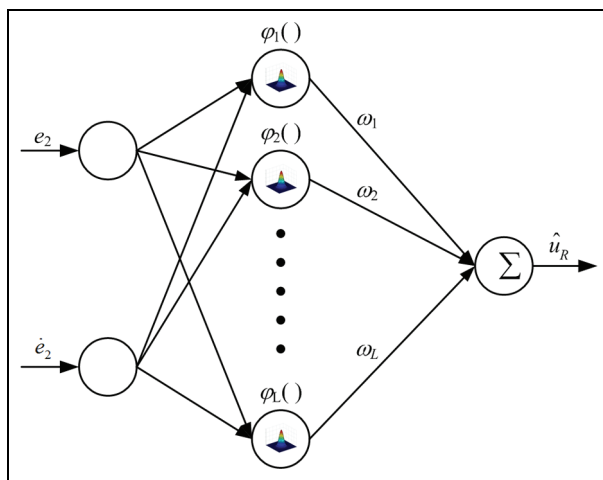


**Figure 4.** Structure of RBFNN.

approximation property, an optimal value of  $u_R^*$  is obtained as follows

$$u_R^* = \sum_{j=1}^L \omega_j^* \varphi_j(\mathbf{E}, \mathbf{c}_j^*, \kappa_j^*) + \varepsilon \quad (20)$$

where  $\omega_j^*$ ,  $\mathbf{c}_j^*$ , and  $\kappa_j^*$  are the optimal parameters of  $\omega_j$ ,  $\mathbf{c}_j$  and  $\kappa_j$ ;  $\varepsilon$  is the minimum reconstructed error, and  $\varepsilon \leq \varepsilon_M$ .  $\varepsilon_M$  is the estimated error bound. To reach the optimal representation, learning algorithm is conducted as follows

$$\begin{cases} \dot{\hat{\omega}}_j = -\eta_1(s_{2g} + s_{2c})\varphi_j \\ \dot{\hat{\mathbf{c}}}_j = -\eta_2(s_{2g} + s_{2c})\hat{\omega}_j\varphi_j\left(\frac{\mathbf{E} - \mathbf{c}_j}{\kappa_j^2}\right) \\ \dot{\hat{\kappa}}_j = -\eta_3(s_{2g} + s_{2c})\hat{\omega}_j\varphi_j\left(\frac{\|\mathbf{E} - \mathbf{c}_j\|^2}{\kappa_j^3}\right) \\ \dot{\hat{\varepsilon}} = -\eta_4(s_{2g} + s_{2c}) \end{cases} \quad (21)$$

where  $\eta_1$ ,  $\eta_2$ ,  $\eta_3$ , and  $\eta_4$  are positive learning gains. Then, the control effort of the improved CSMC with RBFNN is expressed as follows

$$\begin{aligned} u &= \frac{1}{b} [\ddot{\theta}_r - a\dot{\theta}_m + \lambda(2\dot{e}_2 + \lambda e_2 + s_{2g}) - \hat{u}_R - \hat{\varepsilon}] \\ &= \frac{1}{b} \left[ \ddot{\theta}_r - a\dot{\theta}_m + \lambda(2\dot{e}_2 + \lambda e_2 + s_{2g}) - \right. \\ &\quad \left. \sum_{j=1}^L \hat{\omega}_j \exp\left(-\frac{\|\mathbf{E} - \hat{\mathbf{c}}_j\|^2}{2\hat{\kappa}_j^2}\right) - \hat{\varepsilon} \right] \end{aligned} \quad (22)$$

### Stability and convergence analysis

Lyapunov function is used to verify the stability of the CSMC tracking controller with the proposed learning algorithm,<sup>16</sup> which is defined as follows

$$\begin{aligned} V_s &= \frac{1}{2} (s_{2g}^2 + s_{2c}^2) + \frac{1}{2\eta_1} \tilde{\omega}^T \tilde{\omega} + \frac{1}{2\eta_2} \mathbf{E}^T \tilde{\mathbf{c}}^T \tilde{\mathbf{c}} \mathbf{E} \\ &\quad + \frac{1}{2\eta_3} \tilde{\kappa}^T \tilde{\kappa} + \frac{1}{2\eta_4} \tilde{\varepsilon}^2 \end{aligned} \quad (23)$$

where  $\tilde{\omega} = \omega^* - \hat{\omega}$ ,  $\tilde{\mathbf{c}} = \mathbf{c}^* - \hat{\mathbf{c}}$ ,  $\tilde{\kappa} = \kappa^* - \hat{\kappa}$ , and  $\tilde{\varepsilon} = \varepsilon^* - \hat{\varepsilon}$  are the approximate errors of  $\omega$ ,  $\mathbf{c}$ ,  $\kappa$ , and  $\varepsilon$ , respectively. Taking time derivative of equation (23), the following can be obtained

$$\begin{aligned} \dot{V}_s &= s_{2g}\dot{s}_{2g} + s_{2c}\dot{s}_{2c} - \frac{1}{\eta_1} \hat{\omega}^T \tilde{\omega} \\ &\quad - \frac{1}{\eta_2} \mathbf{E}^T \hat{\mathbf{c}}^T \tilde{\mathbf{c}} \mathbf{E} - \frac{1}{\eta_3} \hat{\kappa}^T \tilde{\kappa} - \frac{1}{\eta_4} \dot{\tilde{\varepsilon}} \end{aligned} \quad (24)$$

Substituting equations (13)–(15), (21) and (22) into equation (24), the following can be obtained

$$\begin{aligned}
\dot{V}_s &= (s_{2g} + s_{2c})(\ddot{\theta}_2 + 2\lambda\dot{\theta}_2 + \lambda^2\theta_2 - \lambda s_{2c}) - \frac{1}{\eta_1}\dot{\boldsymbol{\omega}}^T\tilde{\boldsymbol{\omega}} \\
&\quad - \frac{1}{\eta_2}\dot{\mathbf{E}}^T\hat{\mathbf{c}}^T\tilde{\mathbf{c}}\dot{\mathbf{E}} - \frac{1}{\eta_3}\dot{\boldsymbol{\kappa}}^T\tilde{\boldsymbol{\kappa}} - \frac{1}{\eta_4}\dot{\tilde{\varepsilon}}\tilde{\varepsilon} \\
&= (s_{2g} + s_{2c})(\ddot{\theta}_r - a\dot{\theta}_m - bu - \sigma + 2\lambda\dot{\theta}_2 + \lambda^2\theta_2 - \lambda s_{2c}) \\
&\quad - \frac{1}{\eta_1}\dot{\boldsymbol{\omega}}^T\tilde{\boldsymbol{\omega}} - \frac{1}{\eta_2}\dot{\mathbf{E}}^T\hat{\mathbf{c}}^T\tilde{\mathbf{c}}\dot{\mathbf{E}} - \frac{1}{\eta_3}\dot{\boldsymbol{\kappa}}^T\tilde{\boldsymbol{\kappa}} - \frac{1}{\eta_4}\dot{\tilde{\varepsilon}}\tilde{\varepsilon} \\
&= (s_{2g} + s_{2c})[-\lambda(s_{2g} + s_{2c}) + \dot{\boldsymbol{\omega}}^T\boldsymbol{\varphi}(\mathbf{E}, \hat{\mathbf{c}}, \tilde{\boldsymbol{\kappa}}) \\
&\quad - \boldsymbol{\omega}^{*T}\boldsymbol{\varphi}(\mathbf{E}, \mathbf{c}^*, \boldsymbol{\kappa}^*) - \tilde{\varepsilon}] \\
&\quad - \frac{1}{\eta_1}\dot{\boldsymbol{\omega}}^T\tilde{\boldsymbol{\omega}} - \frac{1}{\eta_2}\dot{\mathbf{E}}^T\hat{\mathbf{c}}^T\tilde{\mathbf{c}}\dot{\mathbf{E}} - \frac{1}{\eta_3}\dot{\boldsymbol{\kappa}}^T\tilde{\boldsymbol{\kappa}} - \frac{1}{\eta_4}\dot{\tilde{\varepsilon}}\tilde{\varepsilon} \\
&= -\lambda(s_{2g} + s_{2c})^2 \leqslant 0
\end{aligned} \tag{25}$$

So that Lyapunov function  $V_s$  is proved to be negative semidefinite, which implied that the CSMC  $s_{2g}$  and  $s_{2c}$  are bounded, and it can be presented by

$$\int_0^t \lambda(s_{2g} + s_{2c})d\tau \leqslant V_s(s_{2g}(0), s_{2c}(0)) - V_s(s_{2g}(t), s_{2c}(t)) \tag{26}$$

for  $\dot{V}_s(s_{2g}(t), s_{2c}(t)) \leqslant 0$ , refer to Barbalat's lemma,<sup>29</sup> and that

$$\lim_{t \rightarrow \infty} \lambda(s_{2g} + s_{2c})^2 = 0 \tag{27}$$

So that  $s_{2g}$  and  $s_{2c}$  will converge to zero and then the proposed CSMC tracking controller is verified to be asymptotically stable.

## Experimental validation

### Experimental hardware and forming process

In order to validate the effectiveness of the proposed servo control system in practice, experimental hardware is constructed as shown in Figure 5. A 370 kN prototype of the double toggle mechanical press has been fabricated, while a YASKAWA servo motor is used to drive the press, and a linear grating scale is attached to the punch to measure its position. The proposed servo control system is established in the industrial computer on the console desk. The main technical parameters of the experimental hardware are listed in Table 1. Compound blanking and drawing processes for two different material sheets, carbon steel and stainless steel, are carried out. The process involves blanking the sheet to a circular piece and then drawing it to a cup shape. According to the plastic forming theory, low speed of the punch driving the upper die is required to reduce the deformation resistance in the forming stage. So that the punch trajectories should be optimally designed for different materials and drawing depth.<sup>30</sup> In this article, a general Bezier model is applied for trajectory planning that the punch position curve can be expressed as follows

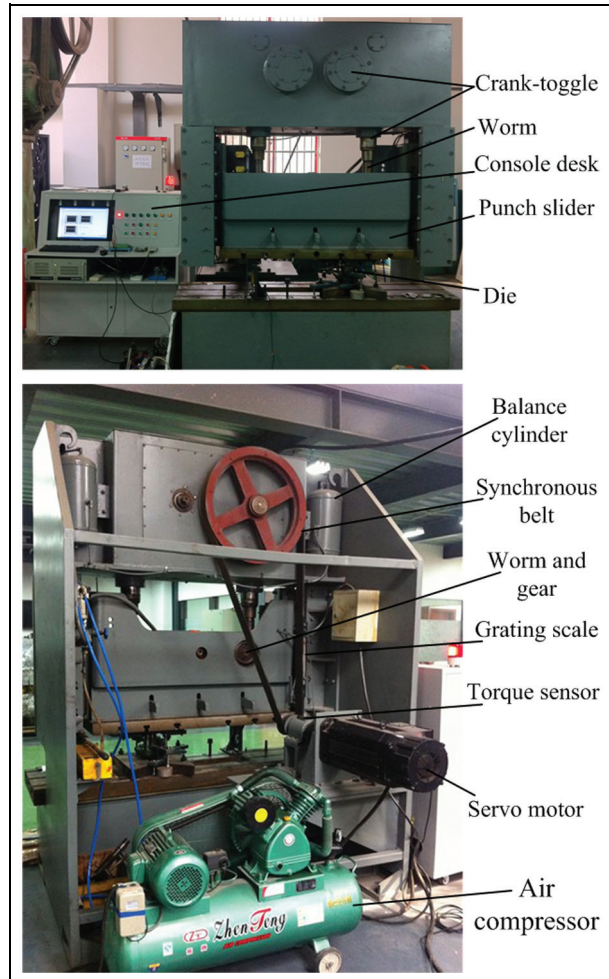


**Figure 5.** Experimental hardware of the mechanical press servo system.

$$D_{sy}(t) = \sum_{i=0}^n D_i B_{i,n}(t) \tag{28}$$

and  $B_{i,n}(t)$  is a  $n$ -time Bernstein basis function

$$B_{i,n}(t) = \frac{n!}{i!(n-i)!} t^i (1-t)^{n-i}, \quad t \in [0, 1] \tag{29}$$

where  $t$  is the dimensionless time on a rotating cycle;  $D_0, D_1, \dots, D_n$  are the control points of the curve; and  $D_0$  and  $D_n$  are the lowest and highest points, respectively. In this article,  $n$  is set to 10.

In the mechanical press, the vibration is caused by the inertial force which is generated by the acceleration of the punch when the workpiece is under processing. Therefore, the optimization purpose of the drawing processing is to minimize the peak of the slider acceleration  $peak(A_{sy}(t))$  which is defined as the objective function

$$\min : f(D_1, \dots, D_{n-1}) = peak\left(\frac{d^2 D_{sy}(t)}{dt^2}\right) \tag{30}$$

Then, the punch motional curves automatically meet the requirements of continuance

**Table I.** Technical parameters of the experimental hardware.

Components	Parameters	Quantities
Mechanical press prototype	Nominal pressure	370 kN
	Nominal pressure stroke	4 mm
	Punch stroke	90 mm
	Maximum die height	250 mm
Servo motor	Die height adjustment	90 mm
	Rated power	22 kW
Torque sensor	Rated torque	256 N m
	Measuring range	0–500 N m
Linear grating scale	Resolution	5 $\mu\text{m}$
Motion control card	Servo update rate	500 $\mu\text{s}$
Data acquisition card	Sampling interval	100 $\mu\text{s}$

$$p_1(D_1, \dots, D_{n-1}) = \frac{dD_{sy}(t)}{dt} \Big|_{t=1} - \frac{dD_{sy}(t)}{dt} \Big|_{t=0} = 0 \quad (31)$$

$$p_2(D_1, \dots, D_{n-1}) = \frac{d^2D_{sy}(t)}{dt^2} \Big|_{t=1} - \frac{d^2D_{sy}(t)}{dt^2} \Big|_{t=0} = 0 \quad (32)$$

In the drawing process, in order to avoid the forming defects such as wrinkle and rupture, one important way is to control the speed of plasticity flow of the semifinished materials. That means, it should be ensured that the punch velocity is approximately equal in the range of the starting point to the end point of the forming process. The equation is expressed as

$$v_{s-e}(D_1, \dots, D_{n-1}) = \frac{\int_{D_s}^{D_e} \left| \frac{dD_{sy}(t)}{dt} - v_{s-Ds} \right| dt}{t(D_e) - t(D_s)} - \varepsilon < 0 \quad (33)$$

where  $\varepsilon$  is a very small value compared with the difference of the punch velocity.  $D_s$  and  $D_e$  are the starting point and the end point of the drawing processing, respectively.  $v_{s-Ds}$  is the punch velocity at the  $D_s$  point, which is limited in a certain speed range for different materials. For example, carbon steel is from 0.092 to 0.253 m/s, stainless steel is from 0.152 to 0.203 m/s, and aluminum alloy is from 0.888 to 1.017 m/s.<sup>31</sup>

In order to achieve the minimization in equation (30), a flexible tolerance genetic algorithm, which is proposed by Shang et al.,<sup>8</sup> is used to calculate the optimal solution ( $D_1, D_2, \dots, D_{n-1}$ ) from equations (30) to (33). Then, substituting the optimal solution into equation (28), the corresponding punch trajectory can be obtained.

### Experimental results

In order to reflect the tracking accuracy and robustness of the proposed CSMC with RBFNN estimator (CSMC-RBFNN), two existing controllers are conducted to compare: a same CSMC without RBFNN and a conventional SMC with a FC (SMC-FC), as

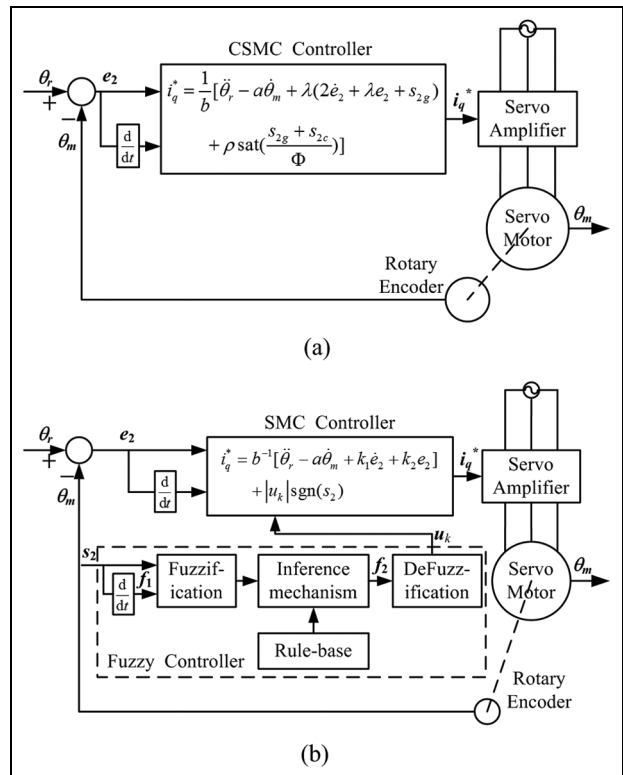


**Figure 6.** Two existing controllers for comparison: (a) conventional CSMC without RBFNN and (b) conventional SMC with fuzzy control.

shown in Figure 6. The forming process of the two materials is implemented with the three controllers, and the parameters of the three controllers are set as follows:

CSMC:  $\lambda = 7.5$ ,  $\rho = 2950$ ,  $\Phi = 0.005$ ;  
SMC-FC:  $k_1 = 15$ ,  $k_2 = 100$ ,  $f_1 = 12$ ,  $f_2 = 3200$ ;  
CSMC-RBFNN:  $\lambda = 7.5$ ,  $\eta_1 = 0.0005$ ,  $\eta_2 = 0.0002$ ,  $\eta_3 = 0.0001$ ,  $\eta_4 = 0.0001$ .

where  $k_1$  and  $k_2$  are the differential gain and proportional gain of the switching function;  $f_1$  and  $f_2$  are the input gain and output gain of the fuzzy controller.

Referring to the carbon steel forming, trajectory response, tracking error, and torque effort of the three controllers are indicated in Figures 7–9, respectively. It can be seen that controlled by the CSMC, large tracking errors and intense chattering of the torque effort occur, that is, because the switching gain is set too large, equal to the upper bound of the lumped uncertainty. When controlled by the SMC-FC, smaller tracking error and chattering can be obtained with the fuzzy compensator, as shown in Figure 8, but the dynamic response of the torque effort is not sufficient, and it would be exhibited on the forming shape of the workpiece. In contrast, the CSMC-RBFNN presents minimum tracking errors and chattering, as shown in Figure 9, and the dynamic response of the torque effort was favorable.

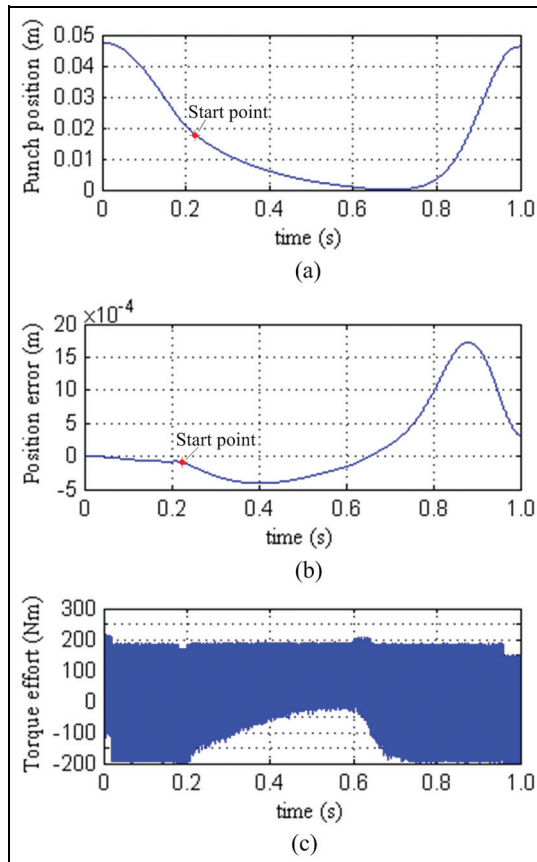


**Figure 7.** Experimental results of CSMC in carbon steel sheet forming process: (a) trajectory response, (b) tracking error, and (c) torque effort.

Furthermore, in order to compare the control performance and forming quality statistically, the forming processes are conducted 15 times independently by each controller. The statistical results of the tracking errors are listed in Table 2. Compared with the CSMC and the SMC-FC, the statistical errors are much reduced when controlled by the proposed CSMC-RBFNN. Thus, it can precisely implement the optimal punch trajectory against the stamping load.

The forming quality of stainless steel with 18 mm drawing depth is compared as shown in Figure 10. Favorable forming shape can be obtained at each time by the proposed CSMC-RBFNN, and the forming

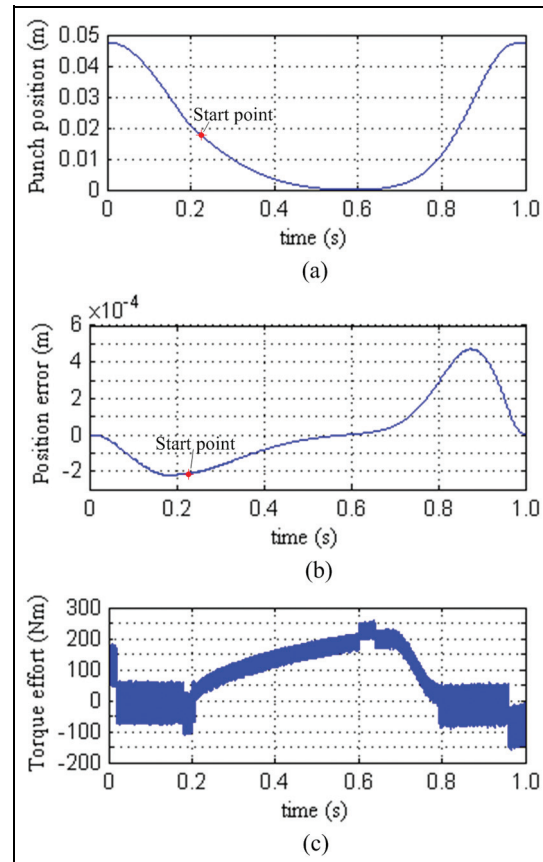


**Figure 8.** Experimental results of SMC-FC in carbon steel sheet forming process: (a) trajectory response, (b) tracking error, and (c) torque effort.

depth errors are all less than 0.5 mm. When controlled by the SMC-FC, wrinkles and edge ruptures are existent five times, it is considered for low learning capability of the torque effort with the FC against the blank holding force and the friction factor, which occurs mechanical vibration in the forming process. When controlled by the CSMC, serious wrinkles and drawing fractures appear on the workpieces, and the press vibrates intensely during the forming process. Consequently, a flexible and precise output torque control has a significant influence on the forming results, and it can control the punch trajectory stably against loading disturbances in the forming process and

**Table 2.** Tracking error performances of the three controllers.

Errors (mm)	Cases					
	CSMC		SMC-FC		CSMC-RBFNN	
	Carbon steel	Stainless steel	Carbon steel	Stainless steel	Carbon steel	Stainless steel
Maximum $E_M$	1.722	1.714	0.471	0.548	0.151	0.173
Average $E_A$	0.169	0.174	0.0164	0.0172	0.0154	0.0169
Standard deviation $E_S$	0.616	0.643	0.192	0.261	0.0590	0.0722

CSMC: complementary sliding-mode control; SMC-FC: sliding-mode control with fuzzy control; CSMC-RBFNN: complementary sliding-mode control with radial basis function neural network.

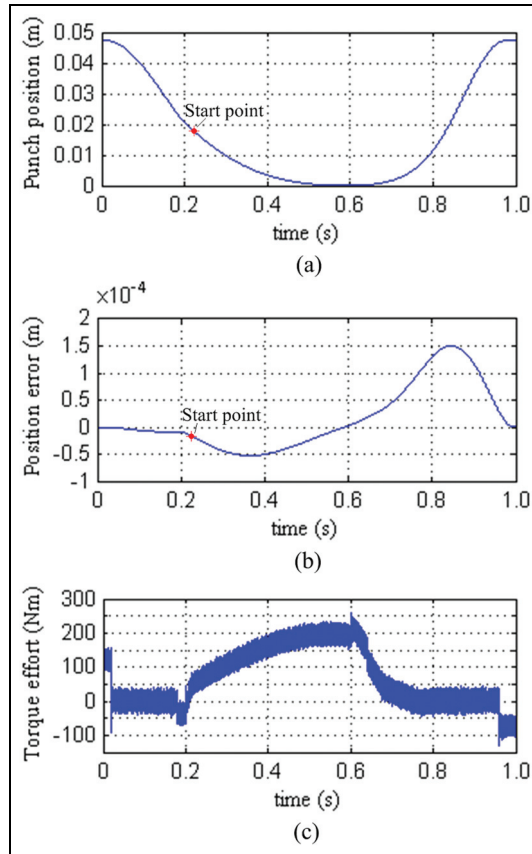


**Figure 9.** Experimental results of CSMC-RBFNN in carbon steel sheet forming process: (a) trajectory response, (b) tracking error, and (c) torque effort.

balance the deformation resistance and the blank holding force adaptively to avoid additional vibrations and frictions.

A 20-mm drawing process of carbon steel controlled by the proposed CSMC-RBFNN is conducted and the workpieces are shown in Figure 11, and the forming shape is well at each time and the forming depth errors are all less than 0.5 mm. Therefore, the statistical results validate that the proposed CSMC-RBFNN exhibited optimum forming quality with different materials.

Combined with the CSMC-RBFNN, the SMC compensator is used to compensate the punch position error and the control gains are optimized by trials. Figure 12 shows the outputs of the SMC compensator in the carbon steel sheet 18 mm drawing process; and it can be seen that the position error is reduced obviously compared with the tracking error that only CSMC-RBFNN is conducted, and the steady-state is guaranteed to be zero. So that combined with the commands from the feedforward controller, punch trajectory with individual drawing depth can be achieved accurately, and favorable forming results can be obtained with different drawing depth, as shown in Figure 13. In summary, the proposed hybrid-loop servo control system exhibits sufficient capability to implement flexible forming processes on the double toggle mechanical press.



**Figure 10.** Workpieces of 18 mm drawing processes of stainless steel with the three controllers: (a) CSMC, (b) SMC-FC, and (c) CSMC-RBFNN.

## Conclusion

In this article, a hybrid-loop servo control system is proposed for realizing various flexible forming processes on a double toggle mechanical press. Accurate control of punch trajectory is required against considerable stamping load disturbances, so that SMC and NNC techniques are used. SMC with proportional switching control law is used to compensate the punch position error, CSMC combined with RBFNN is used to feedback control the servo motor, and the RBFNN is applied to estimate the lumped uncertainty mainly caused by the stamping load. Experimental validations of a compound blanking and drawing process have been carried out. The experimental results show that the proposed methods can implement flexible punch



**Figure 11.** Workpieces of 20 mm drawing processes of carbon steel with the proposed CSMC-RBFNN.

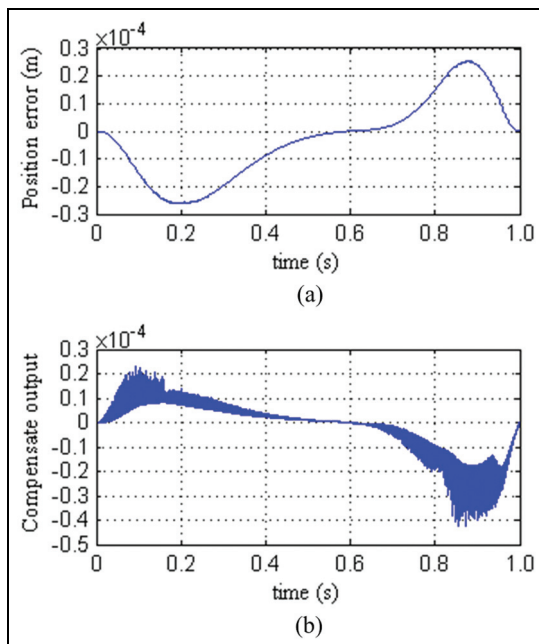


**Figure 12.** Experimental results of the SMC position error compensator in carbon steel sheet forming process: (a) position error and (b) compensate output.



**Figure 13.** Workpieces with different drawing depth.

trajectories and achieve favorable forming quality with different materials and drawing depth. Therefore, this article contributes to the servo control system establishment of the double toggle mechanical press to realize

flexible forming process. Moreover, forming process with different operating parameters can be researched to obtain the optimal performance, and the concept of the hybrid-loop servo control can be extended to any other mechanical servo press.

#### Declaration of conflicting interests

The author(s) declared no potential conflicts of interest with respect to the research, authorship, and/or publication of this article.

#### Funding

This research work is financially supported by the National Natural Science Foundation of China (Nos 51335009 and 51305333).

#### References

- Osakada K, Mori K, Altan T, et al. Mechanical servo press technology for metal forming. *CIRP Ann: Manuf Techn* 2011; 60: 651–672.
- Osakada K, Matsumoto R, Otsu M, et al. Precision extrusion methods with double axis servo-press using counter pressure. *CIRP Ann: Manuf Techn* 2005; 54(1): 245–248.
- Mori K, Akita K and Abe Y. Springback behaviour in bending of ultra-high-strength steel sheets using CNC servo press. *Int J Mach Tool Manu* 2007; 47(2): 321–325.
- Otsu M, Yamagata C and Osakada K. Reduction of blanking noise by controlling press motion. *CIRP Ann: Manuf Techn* 2003; 52(1): 245–248.
- Tokuz LC and Uyan S. Modeling, simulation and control of a four-bar mechanism with a brushless servo motor. *Mechatronics* 1997; 7(4): 369–383.
- Choi H, Jang D, Ko B, et al. A study on the optimization of a mechanical press drive. *Proc IMechE, Part B: J Engineering Manufacture* 2004; 218(2): 189–196.
- He YP, Zhao SD, Wang J, et al. Working mechanisms of the mechanical press with low-speed forging-stamping. *J Mech Eng* 2006; 42(2): 145–149 (in Chinese).
- Shang WF, Zhao SD and Shen YJ. A flexible tolerance genetic algorithm for optimal problems with nonlinear equality constraints. *Adv Eng Inform* 2009; 23(3): 253–264.
- Song QY, Guo BF and Li J. Drawing motion profile planning and optimizing for heavy servo press. *Int J Adv Manuf Tech* 2013; 69: 2819–2831.
- Jin M, Lee J and Chang PH. Practical nonsingular terminal sliding-mode control of robot manipulators for high-accuracy tracking control. *IEEE T Ind Electron* 2009; 56(9): 3593–3601.
- Shang WF and Zhao SD. A sliding mode flux-linkage controller with integral compensation for switched reluctance motor. *IEEE T Magn* 2009; 45(9): 3322–3328.
- Huang YS and Sung CC. Implementation of sliding mode controller for linear synchronous motors based on direct thrust control theory. *IET Control Theory A* 2010; 4(3): 326–338.
- Su JP and Wang CC. Complementary sliding control of non-linear system. *Int J Control* 2002; 75(5): 360–368.

14. Lin FJ, Chen SY and Huang MS. Adaptive complementary sliding-mode control for thrust active magnetic bearing system. *Control Eng Pract* 2011; 19: 711–722.
15. Wang W and Liu XD. Fuzzy sliding mode control for a class of piezoelectric system with a sliding mode state estimator. *Mechatronics* 2010; 20(6): 712–719.
16. Vu NT, Yu DY and Choi HH. T-S fuzzy-model-based sliding-mode control for surface-mounted permanent magnet synchronous motors considering uncertainties. *IEEE T Ind Electron* 2013; 60(10): 4281–4291.
17. Fei JT and Zhou J. Robust adaptive control of MEMS triaxial gyroscope using fuzzy compensator. *IEEE T Syst Man Cy B* 2012; 42(6): 1599–1607.
18. Karayiannis NB and Randolph-Gips MM. On the construction and training of reformulated radial basis function neural networks. *IEEE T Neural Netw* 2003; 14(4): 835–846.
19. Abiyev RH and Kaynak O. Fuzzy wavelet neural networks for identification and control of dynamic plants - A novel structure and a comparative study. *IEEE T Ind Electron* 2008; 55(8): 3133–3140.
20. Wai RJ and Muthusamy R. Fuzzy-neural-network inherited sliding-mode control for robot manipulator including actuator dynamics. *IEEE T Neural Network Learn Syst* 2013; 24(2): 274–287.
21. Bakkemps B, Kostic D, de Jager B, et al. Learning-based identification and iterative learning control of direct-drive robots. *IEEE T Contr Syst T* 2005; 13(4): 537–549.
22. Lin J and Lian RJ. Hybrid self-organizing fuzzy and radial basis-function neural-network controller for gas-assisted injection molding combination systems. *Mechatronics* 2010; 20(6): 698–711.
23. Fei JT and Ding HF. Adaptive vibration control of microelectromechanical systems triaxial gyroscope using radial basis function sliding mode technique. *Proc IMechE, Part I: J Systems and Control Engineering* 2013; 227(12): 264–269.
24. Fei JT and Ding HF. Adaptive sliding mode control of dynamic system using RBF neural network. *Nonlinear Dynam* 2012; 70(2): 1563–1573.
25. Cheng HL and Pei LT. Experimental study on a hybrid-driven servo press using iterative learning control. *Int J Mach Tool Manu* 2008; 48(2): 209–219.
26. Wei SG, Zhao SD, Zheng JM, et al. Self-tuning dead-zone compensation fuzzy logic controller for a switched-reluctance-motor direct-drive hydraulic press. *Proc IMechE, Part I: J Systems and Control Engineering* 2009; 223(5): 647–656.
27. Cheng PY, Chen PJ and Lin YT. Small mechanical press with double-axis servo system for forming of small metal products. *Int J Adv Manuf Tech* 2013; 68: 2371–2381.
28. Tsang KM and Wang J. Control of a permanent magnet synchronous motor using a second-order non-linear trajectory smoother. *Proc IMechE, Part I: J Systems and Control Engineering* 2005; 219(18): 565–575.
29. Teel AR. Asymptotic convergence from  $L_p$  stability. *IEEE T Automat Contr* 1999; 44(11): 2169–2170.
30. Yan HS and Yeh CC. Integrated kinematic and dynamic designs for variable-speed plate cam mechanisms. *Proc IMechE, Part C: J Mechanical Engineering Science* 2011; 225(1): 194–203.
31. Wick C, Benedict JT and Veilleux RF. *Tool and manufacturing engineers handbook, vol. 1 materials, cold-working & non-tradition technology*. Dearborn, MI: Society of Manufacturing Engineers, 1983, pp.15–63.